Magnetic Levitation and Compression at General Fusion – Experiment and Simulation

Carl Dunlea [1*], Ivan Khalzov [2], Stephen Howard [2], Wade Zawalski [2], Kelly Epp [2], General Fusion Team [2], Chijin Xiao [1], Akira Hirose [1]

[1] University of Saskatchewan, Saskatoon, Canada (* cpd716@mail.usask.ca), [2] General Fusion, Burnaby, BC, Canada

19th International Congress on Plasma Physics, Vancouver, 4-8 June 2018

EXPERIMENT

General Fusion is developing a magnetized target fusion power plant. Implosion of a liquid lithium-lead shell by the action of pistons external to the shell will compress a compact torus to fusion conditions[1]. The SMRT magnetic compression experiment was designed as a repetitive non-destructive test to study plasma physics applicable to magnetic target fusion compression.

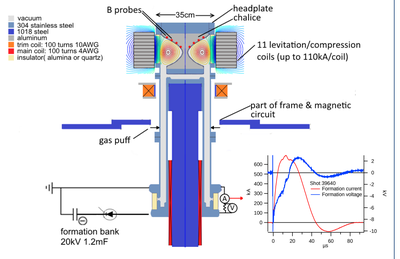

Figure 1: SMRT schematic

A spheromak compact torus (CT) is formed with a magnetized Marshall gun into a containment region with an hour-glass shaped inner flux conserver (the chalice), and an insulating outer wall. The experiment has external coils to keep the CT off the outer wall (levitation) and then rapidly compress it inwards.

Diagnostics included over 20 probes to measure B_α at the CT edge & B_ϕ (shaft current), and thru-CT- chords for laser interferometers (3), optical emission (5), ion-Doppler (2), spectrometers (2), as well as Xray-phosphor imaging.

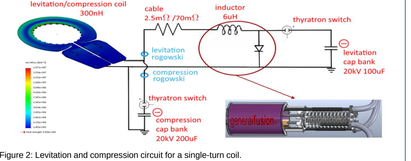

Figure 2: Levitation and compression circuit for a single-turn coil.

Each coil had a separate identical circuit. Unlike the crowbarred levitation currents, compression currents are allowed to ring with the capacitor discharge. Peak CT comp. is achieved at the peak of the 1st half period.

CT Formation into a Levitation Field

- With the original design levitation field profile from 6 coils, CTs were short-lived, up to ~100μs FWHM from poloidal probes at 52mm. In contrast, similar General Fusion (MRT) injectors, without sustainment and with an aluminum outer flux conserver instead of a levitation field had lifetimes greater than 300μs.

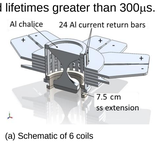

Figure 3: (a) Schematic of 6 coils

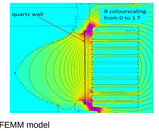

(b) FEMM model
11 coil set - 16kA/coil at 4kHz

- CT lifetime was increased, up to ~160μs, by shortening the ceramic insulator by 7.5cm and adding a steel extension tube (figure 3 (a)).
- The extension mitigated the problems of sputtering of steel at the alumina/steel lower interface, and of CT radiative heat loss due to impurities being added to the plasma as a result of plasma interaction with the insulating wall, especially during the formation process.
- Increasing initial CT flux (ie increasing V_{form} and stuffing field) to the nominal levels associated with MRT CTs did not improve lifetime.

- An insulator with larger internal radius was tried - original ceramic (alumina) replaced with quartz.
- τ_{decay} scales with r^2, so lifetime should have increased from 160μs to ~240μs, but decreased to 120μs - the quartz wall led to even more impurities and further cooling.
- Furthermore, unlike with aluminum and alumina, CT performance with the quartz wall didn't improve very much after Li gettering.

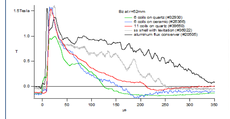

Figure 4: (a) Comparison of B_α at r=52mm

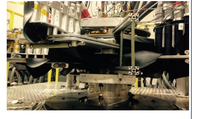

(b) 11 coils on machine

- The setup with 11 coils allowed for formation of higher-flux CTs.
- The absence of gaps outboard of the insulator above and below the coils reduced displacement of the levitation field during CT formation, leading to a reduction of plasma/insulator interaction and impurities.
- Even at increased formation voltage, total spectral power was ~4 times lower with 11 coils.
- CT lifetime was increased ~50%, up to ~190μs, with 11 coils. It is expected that lifetime would increase to ~360μs with a setup with 11 coils on a quartz-radius ceramic wall.

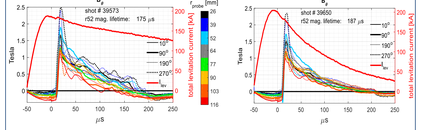

Figure 5: Poloidal field for levitated CT with 11 coils
(a) with 2.5 mΩ cables (b) with 70 mΩ cables

- Adding resistance to the circuit between the main inductors and the coils (figure 2) helped match the decay rate of B_{lev} to that of I_{plasma}.
- This improved on the 'unintentional compression' situation in which a nearly constant levitation flux pushes on a CT which has rapidly decreasing flux.
- A much higher rate of 'good' shots, smoother decays of B_α & B_ϕ, and a ~10% increase in lifetime, was observed with the 70 mΩ cables.

CT Magnetic Compression

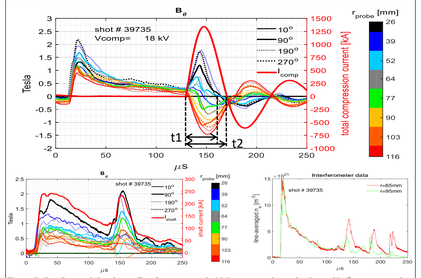

Figure 6: B_{α}, B_{ϕ}, and density profiles for an example high-compression ratio shot, with 'flux conservation parameter' ~0.7. The flux conservation parameter is t1 / t2, where t1 is the average time (over the 2 probes 180° apart at 26mm) from the start of the compression pulse to the time at which the measured B_ϕ falls to 0, and t2 is half-period of the compression current.

- B_ϕ rises by a factor ~10(max) / 7.5(avg), r=26mm probes, at compression, & density (r=65mm interferometer) rises by a factor of 7 (shot #39735).
- Density front generally moves in at 5 to 10 km/sec on compression shots.

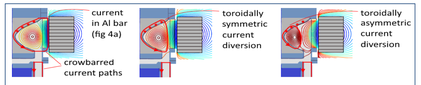

Figure 7: After the 50μs capacitor-driven formation pulse, crowbarred current continues to flow in 2 separate current loops as indicated. External poloidal current, and B_α at probes, rise at compression as the current path shifts to a lower inductance one (central subfigure). Kink instability results in a concentration of diverted current at the kink location. This explains the dip in B_α that is observed at one toroidal angle on many compression shots (eg see Figure 6). Kink can be stabilized by adding toroidal field (shaft current), but is independent of the presence of a conducting outer wall.

- Asymmetric current diversion was also usual towards the end of CT life on levitation-only shots with the low resistance levitation circuit (low level compression), but was not observed on levitation-only shots with the 70 mΩ cables.
- Ideally, as the CT decompresses, the current path returns towards its pre-compression path.
- Flux-conserving compression shots generally exhibited more asymmetric current diversion than non flux-conserving shots, perhaps because the latter destabilized through another mechanism.
- Several shots with ~1ms of sustained ~90kA capacitor-driven shaft current have clear n-odd fluctuations in B_{α}. Increasing sustained current at compression would likely stabilize the kink

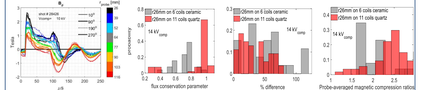

Figure 8: Typical flux-lossy compression shot with 6 coils. Compressional flux conservation, compression symmetry (ie. % difference in mag. comp. ratios at the 2 probes 180° apart at r=26mm), and magnetic compression ratios, were improved with the 11 coil configuration. All data shown here is from shots with compression fired 40-60μs after formation, and at V_{comp} (14kV).

- Vastly improved compressional flux conservation with 11 coils is likely due to the field profile as well as impurity reduction.

Levitated CT lifetimes (Effect of Lithium)

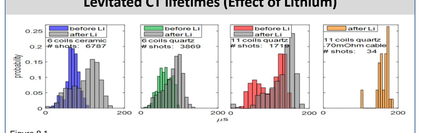

Figure 8.1

- Lithium gettering was more effective on ceramic than on quartz. Only a few shots taken in the most advantageous configuration tested.

SIMULATION

- We developed an energy and toroidal flux conserving finite element axisymmetric MHD code to study CT formation and compression.
- Braginskii MHD equations with anisotropic heat conduction, with constant diffusion coefficients or coefficients based on the Chapman-Enskog-like closures. Option of Bohm diffusion for perpendicular thermal diffusion.
- Isotropic plasma resistivity (Spitzer) and viscosity (Braginskii or constant).
- To simulate plasma / insulating wall interaction, we couple the vacuum field solution in the insulating region to the full MHD solution in the remainder of the domain, while maintaining toroidal flux conservation.
- Simulations can start from vacuum field (formation) or from a Grad-Shafranov equilibrium (GSE).
- Boundary conditions for ψ, pertaining to main, levitation and compression currents are obtained using a FEMM model of the machine geometry.
- Levitation & compression ψ bcs, and, for formation sims, the voltage across the machine electrodes, and, for simulations starting with a GSE, the shaft current, are time-evolved according to shot-dependent experimentally measured signals.
- Simulation of neutral fluid - ion cooling due to plasma–neutral interaction.
- Euler, RK2 and RK4 timestepping. Self-corrective timestep-adjustment.
- Simulated diagnostics for B_α, B_ϕ, ne, Ti , and q profile.
- Convergence studies. GSE and q solutions benchmarked *cf* Corsica.

Energy and Toroidal Flux Conservation

Mass and energy conservation:

$$\dot{\rho} = -\nabla \cdot (\rho \mathbf{v})$$
$$\dot{p} = -\mathbf{v} \cdot \nabla p - \gamma p \nabla \cdot \mathbf{v} + (\gamma - 1)\left(\eta' J^2 + \underline{\pi} : \nabla \mathbf{v} - \nabla \cdot \mathbf{q}\right)$$

The reduced Ohm's law is: $\mathbf{E} + \mathbf{v} \times \mathbf{B} = \eta' \mathbf{J}$. Here $\eta\,[m^2/s] = \frac{\eta'}{\mu_0}$ is the magnetic diffusivity, $\eta'\,[\Omega - m]$ is plasma resitivity. Ohm's law, with Maxwell's eqns., and noting that $\dot{f} = r\dot{B}_\phi$, $\dot{\psi} = r\dot{A}_\phi$, and $\mathbf{E} = -\nabla \mathbf{\Phi}_E - \dot{\mathbf{A}}$, leads, when $\frac{\partial}{\partial \phi} \to 0$ to:

$$\dot{\psi} = \dot{\psi}_{ideal} + \dot{\psi}_\eta = -(\mathbf{v} \cdot \nabla)\psi + \eta \Delta^* \psi$$
$$\dot{f} = \dot{f}_{ideal} + \dot{f}_\eta = r(\nabla \times \mathbf{v} \times \mathbf{B})_\phi + r(-\nabla \times (\eta \nabla \times \mathbf{B}))_\phi$$

Defining the axisymmetric field: $\mathbf{B} = \nabla\psi \times \nabla\phi + f\nabla\phi$, the rate of change of the system's total energy can be expressed as:

$$\dot{U}_{total} = \dot{U}_{KE} + \dot{U}_{TH} + \dot{U}_M = \int \left[\left(\tfrac{1}{2}\dot{\rho}v^2 + \rho\mathbf{v}\cdot\dot{\mathbf{v}}\right) + \frac{\dot{p}}{\gamma - 1} + \frac{1}{2\mu_0}\left(\frac{\partial}{\partial t}\left(\left(\frac{\nabla\psi}{r}\right)^2 + \left(\frac{f}{r}\right)^2\right)\right)\right] dV$$

Expansion (continuous form):

$$\begin{aligned}
\dot{U}_{total} &= \int \nabla \cdot (\Sigma_\alpha (\mathbf{v}_\alpha X_\alpha) + \mathbf{S} + \mathbf{q})\, dV \qquad (\mathbf{S} = \mathbf{E}\times\mathbf{H},\ \mathbf{q} = n\chi\nabla\mathbf{T}) \\
&= \int ((\Sigma_\alpha (\mathbf{v}_\alpha X_\alpha) + \mathbf{S} + \mathbf{q}) \cdot \mathbf{ds} \\
&= \int (\mathbf{S} + \mathbf{q}) \cdot \mathbf{ds} = \Gamma_b \qquad (v_\alpha|_b = 0) \\
&= 0 \qquad (\chi|_b = \psi|_b = (\nabla_\perp f)|_b = 0)
\end{aligned}$$

An expression for $\dot{U}_{total}$, in terms of the discrete, grid-based differential operators and fields, is found using various matrix transpose identities along with inherent properties of the operators. We use the identities that $-\dot{U}_{M\theta\eta} = \dot{U}_{TH\partial\eta}$ (ie rate of loss of magnetic energy associated with poloidal field due to resistive decay of toroidal currents = rate of increase of thermal energy due to Ohmic heating by toroidal currents), and $-\dot{U}_{M\partial\eta} = \dot{U}_{TH\theta\eta}$:

$$\dot{U}_{total} = \underline{dV}' * \left[\Sigma_\alpha \left(\underline{v}_\alpha \circ \left(\underline{\rho} \circ \underline{\dot{v}}_\alpha + \underline{X1}_\alpha + \underline{X2}_\alpha + ... + \underline{Xn}_\alpha\right)\right) + (\nabla \cdot \mathbf{q})_{discrete-form}\right]$$

$\underline{dV} = \frac{2\pi}{3}(\underline{Area} \circ \underline{R})$ ($\{[N_{nodes} \times 1]\}$) is the grid-vector of elemental volumes - dV_i is the volume associated with computation node i. $\underline{v}_\alpha$ is the node-based grid-vector of velocity components ($\alpha \to r, \phi, z$). $n_\alpha + 1$ is the total number of terms ($\rho \circ \dot{v}_\alpha$ and $\underline{Xn}_\alpha$) with the coefficient v_α that are obtained in discretized form for the rate of change of total energy. Setting each of the 3 expressions $\rho \circ \dot{v}_\alpha + \underline{X1}_\alpha + \underline{X2}_\alpha + ... + \underline{Xn}_\alpha$ to zero, we obtain a discrete form of the momentum equation that ensures, with appropriate boundary conditions, that total energy is conserved in the limit of no thermal diffusion. Continuous form:

$$\dot{\mathbf{v}} = -\mathbf{v} \cdot \nabla \mathbf{v} + \frac{1}{\rho}(-\nabla p + \mathbf{J} \times \mathbf{B} + \nabla \cdot \underline{\pi})$$

For conservation of Φ_{ideal} we want: $\dot{\Phi}_{ideal} = \int \frac{\dot{I}_{ideal}}{r} dr dz = \frac{1}{2\pi} \int \frac{\dot{I}_{ideal}}{r^2} dV = 0$.
$\frac{\dot{I}_{ideal}}{r} = \frac{1}{r}(\nabla \times \mathbf{v} \times \mathbf{B})_\phi$, this can be rearranged:
$\frac{\dot{I}_{ideal}}{r^2} = -\frac{1}{r}\frac{\partial}{\partial r}\left(\frac{v_z f}{r} + \frac{v_\alpha}{r}\frac{\partial \psi}{\partial z}\right) - \frac{1}{r}\frac{\partial}{\partial z}\left(\frac{v_z f}{r} - \frac{v_\alpha}{r}\frac{\partial \psi}{\partial r}\right) = \nabla \cdot \mathbf{C} \Rightarrow \dot{\Phi}_{ideal} = \frac{1}{2\pi}\int \mathbf{C} \cdot \mathbf{ds}$.
where $C_r = -\frac{1}{r}\left(\frac{v_z f}{r} + \frac{v_\alpha}{r}\frac{\partial \psi}{\partial z}\right)$, and $C_z = -\frac{1}{r}\left(\frac{v_z f}{r} - \frac{v_\alpha}{r}\frac{\partial \psi}{\partial r}\right)$
With bcs: $v_\alpha|_b \to 0 \Rightarrow C_\alpha|_b \to 0 \Rightarrow \dot{\Phi}_{ideal} = 0$.
Conservation of Φ_η where $\dot{\Phi}_\eta = r(-\nabla \times (\eta \nabla \times \mathbf{B}))_\phi$, is achieved using the inherent properties of the code's 2^{nd} order differential operators, which preserve $(\nabla_\perp f)|_b = 0$ when $(\nabla_\perp f)|_b = 0$ initially.

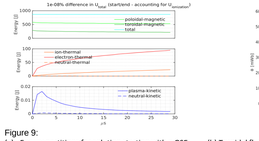

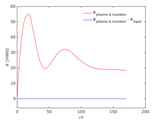

Figure 9:
(a) Energy partitions for solution starting with a GSE; bcs: $(\chi|_b = \psi|_b = (\nabla_\perp f)|_b = 0)$ (b) Toroidal flux conservation (formation run)

Plasma–Neutral Interactions

Neutrals lead to ion cooling, can match ion-Doppler measurement:

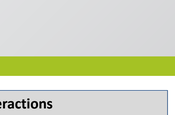

$$i^+ + n \to n + i^+$$
$$e^- + n \to i^+ + 2e^- - \phi_{ion}$$
$$e^- + i^+ \to n + h\nu_p$$

Boltzmann eqn.: $\frac{\partial f_\alpha}{\partial t} + \mathbf{v} \cdot \nabla_{\mathbf{x}} f_\alpha + \frac{q_\alpha}{m_\alpha}(\mathbf{E} + \mathbf{v} \times \mathbf{B}) \cdot \nabla_{\mathbf{v}} f_\alpha = \frac{\partial f_\alpha}{\partial t}|_{collisions} = C_\alpha^{recat.,\,react.}$

Can neglect charged-neutral scattering terms.

For reactive ionization & recombination terms, can take 0^{th}, 1^{st}, 2^{nd} moments, or just assess effects of the sources on momentum & energy.

Take 1^{st}, 2^{nd} moments of CX collision operator for reactive CX terms in momentum and energy conservation equations.

eg $\Gamma_e^{ion} = \int C_e^{ion} d^3V = -n_n n_e < \sigma_{ion} V_e >$, $\Gamma_e^{rec} = \int C_e^{rec} d^3V = -n_i n_e < \sigma_{rec} V_e >$
Rate parameters $< \sigma_{ion} V_e >$, $< \sigma_{rec} V_e >$, and CX cross-section $\sigma_{cx-H}(V_{cx})$ from data-fits ($Voronov,\ McWhirter,\ Barnett$)

Including ionization & recombination and charge exchange terms, as well as neutral source terms, and density diffusion (correction terms D_{ne} and D_{nnc} to maintain energy and momentum conservation), we obtain:

$$\dot{n}_i = -\nabla \cdot (n\mathbf{v})_i + \Gamma_i^{ion} - \Gamma_i^{rec} + D_{ni} \nabla^2 n_i$$
$$\dot{\mathbf{v}}_i = -\mathbf{v} \cdot \nabla \mathbf{v}_i + \frac{1}{\rho_i}\left(-\nabla p_i - \nabla \cdot \underline{\pi}_i + J \times \mathbf{B} - \Gamma_i^{ion} m_i \mathbf{v}_{in} - \Gamma_i^{cx} m_i \mathbf{v}_{in} - \mathbf{R}_{ni}^{cx} + \mathbf{R}_{in}^{cx}\right) + D_{ni} \cdot$$
$$\dot{p}_i = -\mathbf{v} \cdot \nabla p_i - \gamma p_i \nabla \cdot \mathbf{v} + (\gamma - 1)\left(-\underline{\pi}_i : \nabla \mathbf{v} - \nabla \cdot \mathbf{q}_i + Q_{ie} + \Gamma_i^{ion} \tfrac{1}{2} m_i v_{in}^2 + Q_{in}^{ion} - Q_i^{rec}\right.$$
$$\left. - \mathbf{R}_{in}^{cx} \cdot \mathbf{v}_{in} + Q_{in}^{cx} - Q_{ni}^{cx} + \Gamma_i^{cx} \tfrac{1}{2} m_i v_{in}^2\right)$$
$$\dot{p}_e = -\mathbf{v} \cdot \nabla p_e - \gamma p_e \nabla \cdot \mathbf{v} + (\gamma - 1)\left(-\nabla \cdot \mathbf{q}_e - Q_{ie} + \eta' J^2 - \Gamma_i^{ion} \varepsilon_{ion} - Q_i^{rec}\right)$$
$$\dot{n}_n = \nabla \cdot (n_n \mathbf{v}_n) - \Lambda^{rec} - \Gamma_n^{ion} + \Gamma_n^{rec} + \Gamma_n^{cx} + D_{nn} \nabla^2 n_n$$
$$\dot{\mathbf{v}}_n = -\mathbf{v}_n \cdot \nabla \mathbf{v}_n + \frac{1}{\rho_n}\left(-\nabla p_n - \nabla \cdot \underline{\pi}_n + \Gamma_n^{rec} m_i \mathbf{v}_{in} - \mathbf{R}_{ni}^{cx} + (1 - \lambda)(\mathbf{R}_{in}^{cx} + \Gamma^{cx} m_i \mathbf{v}_{in}) + \Gamma_n^{cx} m_n (\mathbf{v}_{n0} - \mathbf{v}_n)\right) + D_{nn} \cdot$$
$$\dot{p}_n = -\mathbf{v}_n \cdot \nabla p_n - \gamma p_n \nabla \cdot \mathbf{v}_n + (\gamma - 1)\left(-\underline{\pi}_n : \nabla \mathbf{v}_n - \nabla \cdot \mathbf{q}_n - Q_{ni}^{ion} + \Gamma_n^{ion} \tfrac{1}{2} m_i v_{in}^2 + Q_i^{rec} + Q_e^{rec}\right.$$
$$\left. + (1 - \lambda)(\mathbf{R}_{ni}^{cx} \cdot \mathbf{v}_{in} + \Gamma^{cx} \tfrac{1}{2} m_i v_{in}^2 + Q_{ni}^{cx}) - Q_{in}^{cx} + \Gamma_n^{cx} \tfrac{1}{2} m_n (\mathbf{v}_{n0} - \mathbf{v}_{n0})^2\right) + \varepsilon_n^{rec} \Gamma_{n0}^{ion}$$

CT Formation

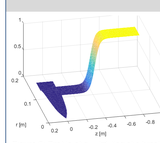

Figure 9: Profile of $q_{form}(z)$ (logistic function)

$$F_{Form}(z,t) = -\int_0^t V_{Form}(t')\, dt' \frac{gForm(z)}{\int \frac{gForm(z)}{r} dr\, dz}$$

Initial particle density is concentrated around the gas-puff location. Assume initial radial current through the high-density region. $V_{form}(t)$ is from experiment. $F_{form}(z,t)$ is added to rhs_f at each timestep.

Model for Insulating Region

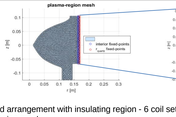

Figure 10: Grid arrangement with insulating region - 6 coil setup
(a) Plasma-region mesh (b) Insulating region

Use $\underline{\psi}_{vac(interior)}(t) = -\left(\underline{\Delta}_{ii}^*\right)^{-1} * \underline{\Delta}_{ib}^* * \underline{\psi}_{vac(b)}(t)$ to solve for ψ_{vac} at nodes inside the insulating region comprised of the outer wall and air between wall and coil-stack. For $\underline{\psi}_{vac(b)}(t)$, use $\psi_{lev/comp(FEMM)}$, scaled with experimentally measured $I_{lev/comp}(t)$, and overwrite with $\psi_{plasma}(t)$ at the interior fixed points (o). Over-write $\underline{\psi}_{plasma(b)}(t)$ at r_{quartz} fixed points (o). Special care was taken to calculate $f_{plasma(b)}(t)$ at r_{quartz} fixed points (o), in order to maintain $\dot{\Phi}_{tot} = 0$.

REFERENCES

1) M. Laberge, et al. *Acoustically driven Magnetized Target Fusion*, Fusion Engineering (SOFE), 2013 IEEE 25th Symposium on, pp.1-7, 10-14 June 2013; doi: 10.1109/SOFE.2013.6635495
2) E.T. Meier, U. Schumak, Physics of Plasmas 19, 072508 (2012)

ACKNOWLEDGEMENTS

Funding provided in part by University of Saskatchewan, General Fusion, NSERC, and MITACS, Canada

Simulation Results

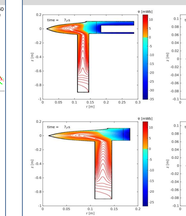

Figure 11: ψ and f contours for 6-coil and 11-coil configurations. Forming CT plasma is held off the wall with 11 coil configuration. Ions gyrorotating around and streaming along B_α lines impact the wall and sputter impurities into the plasma in 6 coil system. The increased levitation field required to minimise interaction with the 6 coil configuration causes the forming CT to be distorted & to shrink during bubble-in at $7\mu s$. Increasing field further can block entry to the confinement area - that was not an issue with 11 coils. Contours of ψ indicate direction of B_α, contours of f indicate direction of J_α. f is constant along the insulating part of the boundary where current is parallel to the wall. Simulation run parameters included:
$\chi_\parallel^i = 1500$, $\chi_\perp^i = 4000$, $\chi_\perp^e = 100$, $\chi_\perp^n = 220\ [m^2/s]$, $n_0 = 3e20$, $n_n|_{t=0} = 5e19\ [m^{-3}]$, $D_p = 100\ [m^2/s]$,
$\nu = 700\ [m^2/s]$, $T_e|_{t=0} = T_i|_{t=0} = 0.02eV$, h_0(triangle size)= 2[mm]
$V_{form} = 166V$, $166A$/coil for 11 coil setup, $31kA$/coil for 6 coil setup.), $t_{main} = 70A$, $R_{cable} = 70m\Omega$

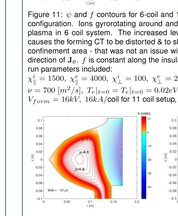

Figure 12: Various fields during compression, 11-coil configuration. Input parameters are as displayed below figure 11, except that $\chi_\perp^i = 10000$, $\chi_\perp^e = 7000$, $\chi_\perp^n = 120$, and $\chi_\perp^n = 50\ [m^2/s]$. $\tau_{decay} = 45\mu s$, and peak compression occurs at $75\mu s$. High values of q around ψ_{axis} are not unusual for 2D simulations as the simulated CTs tend to be very 'hollow', ie have both poloidal and toroidal currents concentrated on the outside of the CT. Ultimately, the simulation is 2D and neglects inherently 3D dissipation associated with turbulent transport. q dips below 1 at the LCFS at $60\mu s$ and the region with $q < 1$ extends towards ψ_{axis} as the compression proceeds. The Kruskal-Shafranov limit is that $q > 1$ for stability against kink mode, which could be stabilized with additional shaft current. The contours of f indicate how, at compression, crowbarred shaft current flows perpendicular to the conducting parts of the boundary, consistent with the boundary condition ($\nabla_\perp f|_b = 0$. The kink-type compressional instability discussed at figure 7 can't be reproduced in the 2D simulation, but this depiction clarifies the mechanism that may cause it to occur.

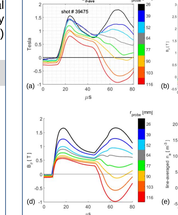

Figure 13: (a), (d): good match for B_α for shot #39475, which had a 'flux conservation parameter' ~1. (b): B_ϕ for simulation, with $\chi_\perp$ as in figure 11 and 70 $m\Omega$ cables, compares well with shot #39650 (figure 5(b)). (e): Line-averaged simulated electron density compares reasonably well with interferometer data (shot #39475). (c) ,(f): B_ϕ *cf* shot #39735 (figure (6)), and ψ contours just before reconnection of the poloidal field associated with the 1^{st} negative polarity CT (induced when I_{comp} rings negative for the 1^{st} time) with B_{comp}, as I_{comp} goes positive again.

CONCLUSIONS

- Reducing plasma–wall interaction and consequent impurities/radiative cooling with levitation field profile modification led to longer-lived CTs.
- Modified compression field profile improved flux-conservation.
- Lifetime would likely increase to the level seen with a metal wall if the quartz is replaced with a more suitable material.
- Matching the decay rates of I_{lev} & I_{plasma} led to increased good shot repeatability, less frequent MHD instability, and ~10% lifetime increase.
- Additional shaft current is required to stabilize kink.